MICROFICHE REFERENCE LIBRARY

A project of Volunteers in Asia

Optimization and Characteristics of a Sailwing
Windmill Rotor

by: M.D. Maughmer

Published by:
Research Applied to National Needs
National Science Foundation
Washington, DC 20550 USA

Paper copies are $8.00 Ask for accession number
PB-259 898 when ordering.

Available from:
National Technical Information Service
Springfield, VA 22161 USA

Optimization and Characteristics of a Sailwing Windmill Rotor

Princeton Univ, N J Dept of Aerospace and Mechanical Sciences

Prepared for

National Science Foundation, Washington, D C Research Applied to National Needs

Mar 76

BIBLIOGRAPHIC DATA SHEET	1. Report No. NSF/RA-760201	2.	3. Recipient's Accession No. PB-259 898
4. Title and Subtitle Optimization and Characteristics of a Sailwing Windmill Rotor (Final Report, February 1, 1975-January 31, 1976)			5. Report Date March 1976
			6.
7. Author(s) M.D. Maughmer			8. Performing Organization Rept. No. AMS 1297
9. Performing Organization Name and Address Princeton University Department of Aerospace and Mechanical Science Princeton, New Jersey 08540			10. Project/Task/Work Unit No.
			11. Contract/Grant No. GI 41891
12. Sponsoring Organization Name and Address Research Applied to National Needs (RANN) National Science Foundation Washington, D.C. 20550			13. Type of Report & Period Covered Final Report, 2/1/75 – 1/31/76
			14.

15. Supplementary Notes

16. Abstracts Within this fourth and final quarter progress report are comprehensively discussed all of the research efforts undertaken by the Princeton windmill group over the past year. This includes a detailed accounting of the development and operational techniques of the Princeton moving-vehicle windmill testing facility. Also presented is a complete documentation of the performance build-up (Dp_{max} = .06 to Cp_{max} = .40) of a 12 ft. diameter, two-bladed Sailwing rotor. This report further includes an examination of an exploratory research effort directed toward using a small, first-stage, co-axial rotor to augment windmill performance. Finally considered are the results and conclusions of an extensive wind-tunnel test program aimed at a quantitative determination of the aerodynamic penalties associated with numerous simplifications of the basic double-membraned Sailwing cross-section.

17. Key Words and Document Analysis. 17a. Descriptors

Wind Power Generation
Windmills
Rotors
Performance Evaluation
Rotary Wings

17b. Identifiers/Open-Ended Terms

Sailwing Windmill Rotor

17c. COSATI Field Group

18. Availability Statement NTIS	19. Security Class (This Report) UNCLASSIFIED	21. No. of Pages
	20. Security Class (This Page) UNCLASSIFIED	

FORM NTIS-35 (REV. 10-73)   ENDORSED BY ANSI AND UNESCO.   THIS FORM MAY BE REPRODUCED   USCOMM-DC 8265-P74

OPTIMIZATION AND CHARACTERISTICS

OF A SAILWING WINDMILL ROTOR

by

Mark D. Maughmer

March, 1976

AMS Report No. 1297

i (a)

Optimization and Characteristics of a Sailwing Windmill Rotor

by

Mark D. Maughmer

Princeton University

Princeton, New Jersey

08540

March, 1976

Final Report

Covering the period February 1, 1975 to January 31, 1976

Approved by:

Thomas E. Sweeney

Director, Flight Concepts Laboratory

i (*)

ABSTRACT

Within this fourth and final quarter progress report are compre-
hensively discussed all of the research efforts undertaken by the
Princeton windmill group over the past year. This includes a detailed
accounting of the development and operational techniques of the Princeton
moving-vehicle windmill testing facility. Also presented is a complete
documentation of the performance build-up ($Cp_{max} = .05$ to $Cp_{max} = .40$)
of a 12 ft. diameter, two-bladed Sailwing rotor. This report further
includes an examination of an exploratory research effort directed
toward using a small, first-stage, co-axial rotor to augment winomill
performance. Finally considered are the results and conclusions of an
extensive wind-tunnel test program aimed at a quantitative determination
of the aerodynamic penalties associated with numerous simplifications
of the basic double-membraned Sailwing cross-section.

TABLE OF CONTENTS

LIST OF SYMBOLS

b	Wing span
c	Wing or blade section chord length
$\bar{c}_A$	Mean aerodynamic chord
h	Maximum section thickness
h/c	Sectional thickness ratio
t	Sectional thickness ratio h/c
q	Dynamic pressure $(\frac{1}{2}\rho V^2)$
A	Rotor disk area
AR	Wing aspect ratio
C_D	Drag coefficient (D/qS)
C_L	Lift coefficient (L/qS)
C_M	Pitching moment coefficient (M/qcS)
C_p	Power coefficient $(Power/qVA)$
L/D	Lift-to-drag ratio
S	Wing area
V	Free-stream wind velocity
α	Wing angle of attack
β	Blade pitch angle relative to the plane of rotation
β_R	Blade root pitch angle relative to the plane of rotation
β_T	Blade tip pitch angle relative to the plane of rotation
ϵ	Blade twist angle (tip relative to root)
γ	Tip-speed ratio (tip-speed/V)
ρ	Air density
σ	Rotor solidity ratio (Blade Area/Disk Area)

INTRODUCTION

With this finalized and comprehensive report, so ends the efforts
of the Princeton windmill research group for the past year. From all
available information, in the case of the smaller-sized family of wind
machines for which the Princeton group has been, and remains, a strong
proponent, the Sailwing rotor continues to be highly competitive in
performance with its rigid-bladed counterparts and yet enjoys the benefits
of simpler construction and lower costs. It is now the feeling of the
Princeton group that with reasonable performance and understanding of the
Sailwing windmill in hand, further pursuance of our goal, which has been
to optimize the Sailwing rotor, would result in diminishing returns for
the effort. While most certainly the moving-vehicle test facility will
continue to be active in testing and comparing different rotors, it is
doubted whether there is much more to be gained from the systematic
build-up technique that has been employed by the Princeton windmill group
up until now. Thus, the aerodynamic refinement of the Sailwing windmill
is now nearly complete. Although it appears as though it might be
possible to achieve rotor efficiencies of nearly 85% ($Cp = .50$), the
great deal of effort required to obtain those last few percentage points
of improvement can probably be spent more effectively in other areas of
the problem. In particular, it would be most satisfying if the results
that have been obtained up until now were "put to good use" and the
feeling is that the time is now right to proceed toward the practical

utilization of the smaller family of wind generators. The development of individual components has progressed to a point where they are ready to be assembled into a well integrated system and demonstrated as a practical means of power generation. Thus, it is toward these goals that the Princeton group would like to direct the expertise it has developed over the last five years of windmill research.

THE PRINCETON JEEP WINDMILL TESTING FACILITY

Early in the efforts of the windmill research program it became apparent that atmospheric testing was unsuitable for the optimization and rapid development of rotor performance that was the goal of the Princeton undertaking. While such techniques are suitable, and even preferred, in the field testing of wind turbines, where such things as the machine's dynamic response to wind vleocity fluctations can have a dramatic effect on the net power generation when integrated over a long period of time, such techniques are almost useless when an accurate determination of the effect of a single configuration change on rotor performance is desired in a relatively short time period. Thus, the development of a moving-vehicle windmill test-bed, Figures 1-3, was begun. The gradual evolution of this facility has now reached a point of sophistication where a more detailed description than has been given it in the past is justified. Furthermore, it is felt that the development and operation should be more carefully documented so that others desiring to utilize a similar technique might benefit from the Princeton experience. Due to both the reasonably low scatter and the high repeatability of the data collected using the jeep windmill testing facility in its current stage of development, it is doubted whether any significant improvements that are within a reasonable cost are possible.

A) Description of the Test Facility

Central to the performance determination of any wind-turbine is an accurate measurement of the undisturbed free-stream wind velocity.

3

In the case of the Princeton Jeep facility, a number of unsatisfactory
anemometry systems were tried before the successful type shown in the
overall views of the test vehicle, Figures 1-3, was employed. These
attempts included both mechanical vane and hot-wire types until the
"home-made" cup-type anemometer, which was ultimately successful, was
installed. The overall problem in this application is that in addition
to a fairly high degree of sensitivity and accuracy, a reasonably steady
meter reading is required such that it can be easily tracked by the
driver to match the speed of the vehicle to the wind velocity desired.
Both the mechanical and the hot-wire types proved to be too susceptible
to road-bumps to allow accurate speed control. The cup-type, on the
other hand, is insensitive to bumps and gives an extremely steady read-
ing, yet, due to its light-weight, halved ping-pong ball construction,
responds quickly to changes in velocity.

In an attempt to remove the anemometer as much as possible from
the disturbing influence on the flow-field caused by the presence of
the jeep, the anemometer is mounted a considerable distance in front of
the vehicle as seen in Figure 2. The cup portion of the instrument is
used to drive a small DC generator whose signal is transmitted to a
milliammeter mounted on the jeep's steering column within easy sight
of the driver, Figure 4. The initial calibration of this system was
accomplished in the wind-tunnel and, in order to prevent errors, is
verified before each series of tests by recording the time required for
the jeep to travel a given distance and comparing the resulting calcu-
lated velocity to that indicated by the instrument. This procedure has

4

the additional purpose of indicating whether or not the natural winds are within the limit at which meaningful data can be obtained.

Throughout the development of the Jeep windmill testing facility, several methods of loading the windmill were tried, the last and most successful being that of a hydraulically actuated motorcycle disk-brake. The master cylinder and actuating mechanism for this system are mounted at the base of the supporting-tower drag brace and operated by a person sitting in the bed of the Jeep. The brake is applied by turning down the turnbuckle shown in Figure 4. The springs shown in the photograph allow a more steady load to be applied in that they have replaced a displacement signal to the actuator-arm with a constant force signal. The disk-brake itself is shown against the larger radius rotor hub assembly in Figure 5. The amount of torque that is generated by the rotor when the brake is applied is measured by a strain-gage bridge mounted on the horizontal portion of the supporting structure. The signal from the strain gages is monitored on the microammeter, shown in Figure 6. Thus, by watching the meter, a desired amount of braking torque can be administered to the windmill by turning down the turnbuckle an appropriate amount. The braking system is calibrated by locking the disk and noting the meter response to a known applied torque as obtained by hanging weights at a given radius on one of the rotor blades.

The final testing parameter that is required in the determination of windmill performance is rotor RPM. This is easily measured by means of a small tachometer mounted at the rotor hub, the signal from which is sent to a voltmeter, Figure 7, and read by the crew member riding in the

right seat of the Jeep. Calibration of this unit is performed by rotating the hub by means of an electric drill and correlating a strobe light RPM measurement with the given voltmeter deflection.

B) <u>Data Collection</u>

The most important requirement for the collection of data using the Jeep windmill testing facility is that of very light or, preferably, no natural winds. It has been found that a light crosswind of possibly two and certainly three miles-per-hour is sufficient to invalidate a data sample. This requirement for absolute calm test conditions is only met with any regularity in the early dawn, and, thus, most of the Princeton data has been obtained during the couple of hours between first daylight and sunrise.

The actual collection of data using the moving test-bed requires a minimum of three researchers. The driver's duty is to maintain the Jeep's speed constant, according to a predetermined anemometer reading, for each pass down the 3000 ft. Princeton University runway. The man in the right seat is responsible for commanding a given braking torque to be applied, reading the RPM meter, and for recording all of the information required at each datum point on a worksheet, a sample of which is presented in Figure 8. This man has the further responsibility of determining when all of the readings have stabilized sufficiently for a point to be taken. Finally, the man sitting in the bed of the Jeep maintains the torque setting required for a given point by watching the torque-meter and adjusting the brake turnbuckle accordingly.

Finally, it is important that the individuals operating the

6

testing vehicle become experienced at their posts and familar to the various subtleties associated with the experimental facility. The fact that the quality of data samples improved significantly as the experience levels of operators increased has been notably evident throughout the Princeton program.

C) Reduction of Data

In order to ascertain the performance of a windmill, the data that is obtained using the Jeep testing facility is generally reduced and presented in the standard plot of power coefficient, Γ_c, as a function of tip speed ratio, $\mathcal{Y}$. This non-dimensional form of data presentation makes it possible to rapidly evaluate a particular windmill or configuration and compare its operation to that of other designs. For optimization research, such as that performed by the Princeton group, this capability to immediately determine the effect on performance of a single configuration change is obviously of great benefit.

Although ideally all data collection utilizing any moving vehicle test-bed should be conducted in absolute calm conditions, it can be reasonably argued that if the wind is blowing parallel to the test-strip, the tests should still be valid in that the data is reduced on the basis of the indicated airspeed of the vehicle and should be the same velocity as that seen by the windmill. However, after some experimentation, it was found that because of a vertical wind velocity gradient above the test strip (boundary layer), along with the fact that the windmill and the anemometer were not mounted at the same elevation above the ground, such was not the case. Thus, in an effort to extend somewhat the conditions

7

under which useful data could be obtained, a method of correction was developed for those occasions when a light wind was blowing parallel, or nearly parallel, to the test strip. This technique is outlined in Appendix II; however, the result of its use can be seen by comparing Figures 9 and 10. In Figure 9, essentially two separate plots have been generated and depend on whether or not a point was obtained on an upwind or on a downwind data collection pass. The actual corrected performance curve is then shown in Figure 10. Because of the cube relationship of velocity to the determination of power, this curve is shifted more heavily toward the higher curve in Figure 9. All in all, the best data is still that collected in calm air; however, this correction technique has added a little flexibility to the Princeton test program and has prevented a number of early morning efforts from being entirely wasted.

PERFORMANCE BUILD-UP OF THE PRINCETON 12 FT. DIAMETER, TWO-BLADED SAILWING WINDMILL

This phase of the Princeton windmill research program is concerned with the systematic performance "build-up" of a 12 foot diameter, 2-bladed Sailwing rotor. The experiments were designed to determine which configuration elements are necessary in obtaining reasonable performance and which elements can be eliminated with the benefit of lowering the overall cost. In addition, unlike the preceding systematic build-up of a 3-bladed Princeton design (Reference 1), this particular rotor was constructed with the capability of easily optimizing each configuration in both pitch and twist. Thus, it was hoped that such capability would add significant insight toward generalized blade design technology. As a further important point, it should be noted that a two-bladed rotor was chosen for the basic design because of the much greater ease with which configuration changes could be accomplished. In the carefully controlled test environment in which this machine was to be utilized, the dynamic problems of a two-bladed rotor when a rapid change about the azimuth occurs could be effectively eliminated; however, even though such problems are minimal because of the low inertia associated with the light-weight Sailwing blades, the Princeton group does recognize the advantages of and strongly recommends the use of three-bladed machines in nearly any practical field application.

As a concluding note, all of the data presented in this report are finalized results and supersede those contained in the preliminary

9

reports concerning the build-up of this design. Several inconsistencies
in the earlier data, as well as several improvements in the testing
facility, led to the retesting of a number of earlier configurations to
arrive at some slightly modified results, although the overall con-
clusions put forth remain essentially unchanged.

A) Data Presentation and Discussion

The basic Sailwing structure from which all the subsequent con-
figurations were evolved is shown in Figure 12(a), while a detailed
summation of the blade dimensions is presented in Figure 11. The wind-
mill itself consists of a twelve-foot diameter, two-bladed rotor which
is constructed using a tapered tubular leading-edge spar and fixed root
(manually rotatable) and tip members. The blade trailing edge consists
of a cable in tension to which is firmly attached the trailing edge seam
of a Dacron sailcloth envelope. The pronounced catenary arc of the
trailing edge produces chordwise tension in the sail itself which can,
when adequately high in tension, eliminate sail luffing. The remaining
configurations tested in this program are summarized in Figure 12, and
involve the addition of a leading-edge fairing (b), blade-tips (c),
center-body disks (d) and (g), and various types of trailing edge stiff-
eners (e) - (g).

During the actual testing of each configuration, the blade pitch
angle was adjusted until the performance was found to drop-off on either
side of an optimum. Furthermore, each configuration was tested at free-
stream wind velocities of 19.6 ft/sec (13.3 mph) and 31.3 ft/sec (21.3 mph).
Thus, the "non-dimensionality" of the windmill performance parameters is

tested and the rate of performance degradation with increasing wind speeds can be evaluated.

The data for each configuration and wind speed that was evaluated was reduced and used to generate a conventional windmill performance curve that plots power coefficient, C_p, against tip-speed ratio, $\mathcal{M}$. The complete set of curves for the configurations shown in Figure 12 are presented in Figures 13-26. These curves summarize the overall performance of each configuration tested and permit a rapid comparison of one configuration with another.

The performance of the basic windmill, Figure 12(a), is shown in Figure 13. It will, of course, be noted that the maximum power coefficient leaves much to be desired. Although this was somewhat expected from previous Sailwing experience, it was felt that use of a tubular leading-edge should be documented to answer one of the most often posed questions concerning the Sailwing blade design. Also shown in Figure 13 is the blade tip cross-section of this configuration which was the only one with a circular leading-edge tested.

The performance of the configuration shown in Figure 12(b) is recorded in Figures 14 and 15. By the simple addition of a full-span D-tube fairing to the leading-edge, the power coefficient has been increased over five times. This is thought to be due to optimizing the blade sectional shape by improving the fluid flow accelerations around the leading-edge, by moving the point of maximum thickness aft, by increasing the sectional camber by introducing approximately seven degrees of leading-edge droop, and, finally, by significantly reducing the

11

relatively large thickness ratio of each section along the blade span. Also shown in Figure 14 is the blade tip profile that was used on all of the remaining configurations, (b) - (g).

Figures 16 and 17 indicate the effect of the geometric addition of smoothly faired blade tips as shown in Figure 12(c). Although the overall power generated by this configuration was increased over that of the tipless version, it was more than balanced by the increased rotor radius used to non-dimensionalize the power in the form of a power co-efficient. The fact that the power coefficient itself did not improve is somewhat surprising but might be explained by a slight deterioration from the optimum loading distribution along the blade span.

Motivated by previous center-body fairing research performed at Princeton (References 1 and 2), the addition of a center-body disk hav-ing a radius 20% that of the overall blade radius, Figure 12(d), resulted in a small improvement in the overall performance as shown in Figures 18 and 19.

A significant improvement of nearly 20% in rotor power coefficient resulted from the addition of the mid-radius trailing-edge stiffener, Figure 12(e), as shown in the performance curves of Figures 20 and 21. This brace between the leading-edge spar and the trailing-edge cable firmly fixes the trailing-edge cable relative to the primary structure at that point but does not effect the basic catenary arc of the trailing-edge. The addition of the 20% center-body disk to this configuration produced very little change in rotor performance, Figures 22 and 23.

An increase in the geometrical solidity of the rotor is achieved

12

by the configuration shown in Figure 12(f) but resulted in a little noticeable change in perfromance, Figure 24. However, by dividing the original single-catenary arc trailing-edge into two smaller catenaries, the unsupported trailing-edge span is halved with the result of significantly raising the critical velocity threshold at which sail-luffing occurs (Reference 1).

Finally, a 20% center-body disk was employed to obtain the configuration shown in Figure 12(g). This modification resulted in the largest power coefficient that was obtained, $C_p = .40$, for the lower wind speed, Figure 25. The higher wind speed performance is presented in Figure 26.

A summary of the significant parameters indicated in Figures 13 - 26 are given in Table I.

Configuration (As per Figure 12)	V = 19.6 ft/sec			V = 31.3 ft/sec		
	λ max	C_{Pmax}	λ(opt)	λ max	C_{Pmax}	λ(opt)
(a)	4.0	.06	2.8			
(b)	6.7	.32	4.0	6.0	.31	3.4
(c)	7.0	.31	4.1	6.6	.30	3.9
(d)	7.6	.34	4.8	6.6	.31	4.2
(e)	8.0	.37	4.9	7.0	.34	4.1
(e) plus center-body	7.6	.39	4.4	7.0	.33	4.2
(f)	7.3	.37	4.3			
(g)	8.0	.40	4.3	7.1	.36	4.1

TABLE I: Summary of the Significant Parameters Obtained in the Performance Build-up of the 12 ft. Diameter, Two-Bladed Sailwing Windmill Rotor.

13

B) Conclusions

In summarizing the findings of these experiments, it can be fairly stated that a circular leading-edge does not produce a good windmill rotor; however, by the simple adition of a drooped leading·edge fairing, the performance of the Sailwing rotor becomes reasonably good. It can further be stated that the addition of wing tip fairings on this configuration did not improve the overall power coefficient obtained. The installation of a 20% center-body disk did modestly improve the rotor performance while a significant gain in rotor efficiency was obtained by halving the unsupported span of the trailing-edge cable.

If the performance curves in Figures 13-26 are examined in more detail an expected trend is observed in that as the performance of the basic machine improves, the optimum blade root pitch angle decreases from twenty degrees to ten degrees as the tip-speed ratio at which the maximum power coefficient occurs increases from 2.8 to 4.3. Somewhat less expected is that fact that the twist distribution is not particularly critical to the rotor performance providing it is within approximately ten degrees of optimum. This is perhaps due to the fact that in the case of the Sailwing, the ideal hyperbolic twist is only approximated by a linear relationship between the root and tip ribs. Thus, as the mid·span sections are flexible and able to adjust to different inflow conditions, perhaps the actual positioning of the tip relative to the root is less important than how the remaining portions of the blade deform.

Over all of the configurations tested, the effect of increasing the wind velocity from 19.6 ft/sec to 31.3 ft/sec resulted in an average

14

deterioration of approximately eight percent in the maximum power co-
efficient obtainable. While this loss in performance is not considered
crucial, some attention must be given to the fact that this condition
will become more pronounced as the velocity approaches that of the criti-
cal value, for a given trailing-edge cable tension coefficient, at which
sail luffing occurs (Reference 1); however, lest the impression is given
that this effect must be entirely detrimental, it has been suggested that
by careful control of the pertinent parameters, the performance degrada-
tion with increasing wind speed can be used to aid in the prevention of
rotor self-destruction in high winds.

Finally, in comparing the final results of the two-bladed Sail-
wing rotor build-up with those of the three-bladed rotor, Figurs 1 and
2, it was expected that the lower overall solidity ratio of the two-
bladed design would allow it to ultimately achieve larger maximum values
of power coefficient. Thus, it was not only disappointing but somewhat
confounding as well when, in spite of higher corresponding tip-speed
ratios, the two-bladed machine achieved a maximum power coefficient of
.4 and required considerably more effort than the three-bladed design
needed to obtain .44 (Reference 1). While the explanation of this dilem-
ma is obviously tied up in the fact that the three-bladed design has an
overall more optimum induced velocity distribution over the disk area,
this has yet to be determined rigorously. Thus, even though both rotors
are considered excellent when compared to other modern machines, one can
appreciate the fact that there remains a great deal to be learned con-
cerning the aerodynamics of windmill design.

15

MULTI-STAGE WINDMILL TO OBTAIN CENTER-BODY FAIRING BENEFITS

Based solely on the intuitive notion that the improved windmill performance that was realized with the addition of a 20% center-body disk on the 12 ft. diameter, 2-bladed Sailwing rotor could also be successfully achieved by the large pressure drop generated at the rotor-disk center by a small, first-stage rotor mounted co-axially in front of the main rotor, a multi-stage rotor assembly was built and tested, Figures 27 and 28. As there had been virtually no previous experience which such a device, the research was to be of a purely exploratory nature and the prototype assembly was designed to permit a number of operational modes as well as easily incorporated modifications. Specifically, as one could only hypothesize as to the most suitable mode of operation for such a device, the symmetrically sectioned, untwisted blades of the small, up-stream rotor were constructed in such a manner that the pitch could be adjusted to allow rotation in the same direction or in the opposite direction to that of the main rotor. Furthermore, it was possible in the course of testing to apply a variable load to the first stage rotor and, therefore, control its operational tip-speed ratio independently from that of the main rotor. This capability was included because it was not intiutively clear whether the flow field would be most beneficial-ly disturbed with the small rotor free-wheeling, extracting additional energy from the streamtube or, although unlikely, drawing-energy from the main rotor in order to put energy into the center portions of the stream tube so that substantially more working fluid would be diverted to

16

the outboard regions. Obviously, a very broad exploratory program would

be required to determine th° most suitable operating mode and only then

could that configuration be optimized and the overall potential of the

concept evaluated.

A) Data Presentation and Summary

The basic rotor configuration with which the multi-stage wind-

mill experiments were conducted is that of Figure 10(f) but without blade

tips. The baseline performance curve of the test-bed windmill without

the first-stage rotor assembly mounted is presented in Figure 29 and

it is by comparison with this curve that the relative merits of the

various operating modes of the co-axial rotor were determined.

The performance plots of the vairous operational configurations

attempted are presented in Figures 30-34. A summation of the important

points taken from these plots is tabulated in Table II.

Configuration	λ_{max}	c_{pmax}	$\lambda(opt)$
Baseline Windmill	7.3	.36	4.1
Co-axial Rotor: Rotations Synch., Free-wheeling, $\beta = 20°$	7.0	.36	4.1
Co-axial Rotor: Rotations Synch., Intermediate Braking, $\beta = 20°$	6.8	.33	3.9
Co-axial Rotor: Rotations, Synch., Braked Locked, $\beta = 20°$	6.8	.33	4.0
Co-axial Rotor: Counter-rotating Free-wheeling, $\beta = 20°$	7.2	.36	3.8
Co-axial Rotor: Counter-rotating Free-wheeling, $\beta = 5°$	7.2	.35	3.9

TABLE II: Summary of the Significant Parameters Obtained in the Multi-Stage Windmill Rotor Experiments.

17

B) Conclusions

In examining the data presented in Table II, one can only come
to the conclusion that all of the co-axial windmill operating conditions
yielded performances that were either the same or slightly worse than
that of the baseline windmill. In any case, the upstream rotor's effect
appears to be so little that further research efforts were ceased. The
only explanation as to the reason for these disappointing results is
that while the upstream rotor may very well produce a fluid-flow dis-
turbance much like the center-body disk, it also produces and "in-plane"
interference due to the drag of its blades. Thus, any beneficial inter-
ference or additional rotor torque is nullified and the net rotor per-
formance remains essentially unchanged. In any case, on the basis of
these experiments, an overall evaluation of the concept would have to
conclude that a simple center-body disk is not only more effective, but
less costly as well.

WIND TUNNEL INVESTIGATION OF VARIOUS SAILWINC AND SAILVANE CROSS-SECTIONAL PROFILES

The motivation for exploring the aerodynamic characteristics of various Sailwing and Sailvane cross-sections was to determine if simplification or modification of the conventional doubled-membraned Sailwing could yield any economical benefits without causing excessive performance penalties. Thus, a wind tunnel program was undertaken and structured in such a manner as to ascertain the relative magnitudes of the penalties associated with using commercially available streamlined sailboat mast and circular cross-sectioned tubing in place of the Sailwing's D-section leading edge. Furthermore, the importance of the full double membrane was tested by including several sections not utilizing the lower membrane as well as several having only a partial lower membrane. In total, eight wings, identical in all respects except for the section utilized, were tested.

A) Model Description

The tests of the eight different wing profiles, shown in Figure 35, were performed in the Princeton University 4 by 5 foot wind tunnel. The wing planform that was utilized is shown in Figure 36 and characterized by a span, b, of 37.8 inches, a mean aerodynamic chord, $\bar{c}_A$, of 4.5 inches, and a total area, S, of 168 sq. inches. The resulting aspect ratio of the planform, AR = $b^2/b\bar{c}$, is equal to 8.4. Relative to the mean aerodynamic chord length, the sectional thickness ratio, t, is 11.5 percent. The trailing-edge cable tension in the models could be varied and was adjusted to 9.5 lbs and 36 lbs for the experimental results

19

discussed herein. Respectively, these values yield a trailing-edge

cable tension coefficient, C_t of .07 and .28.

B) Test Conditions and Data Reduction

All of the data collected in the series of experiments included

in this report were obtained with the tunnel speed adjusted to yield a

dynamic pressure, q , of 13.0 $lb./ft^2$. Although the corresponding

Reynold's Number, based on the mean aerodynamic chord, can be calculated

to be approximately 250,000,because of the turbulence level in the tunnel,

the aerodynamic data collected is more representative of a higher Reynold's

Number on the order of 750,000.

The mounting of a typical test model in the wind tunnel is shown

in Figure 37. The mounting arrangement permits the wing angle-of-attack

to be adjusted while the tunnel is in operation to any value between -12

and +24 degrees. Thus, force balance data for lift, drag, and pitching

moment were obtained at each two-degree angle increment between the limits.

These data were then reduced to the standard coefficient form and plotted

as a function of the wing angle-of-attack as referenced to the unloaded

(no-wind) orientation of the mean aerodynamic chord. In addition, the

efficiency of each of the wings is summarized in a plot of the lift-to-

drag ratio, L/D, as a function of wing angle-of-attack.

One difficulty with the experimental technique that should be

pointed out is concerned with the fact that all of the drag measurements

are obtained by subtracting a very large tare drag reading from a very

large overall drag reading to obtain the very small drag contribution of

the model. Although this is the common procedure when a limited amount

20

of time and funding are available, it undoubtedly allows small errors in the drag measurement to enter into the experiment. This is not to say that the procedure yields data which is unsuitable for design purposes and it is certainly acceptable for comparative purposes; however, the results obtained in this manner should not be considered absolute.

C. Characteristics of the Sailwing

Because of the flexible nature of the Sailwing, it possesses several unique features that cause it to differ greatly from a conventional rigid wing and it is therefore appropriate to discuss some of these characteristics in relation to the Sailwing's operation. For example, when the Sailwing is at rest (no-wind), the cloth membrane is held taut by the trailing-edge cable and is essentially, except for the leading-edge, a symmetrical section as the upper and lower surfaces experience the same pressure, Figure 37. As the wing becomes operational in a lifting orientation (wind-on), the asymmetrical pressure distribution that is established between the upper and lower surfaces causes the membrane (or membranes) to deform away from the high pressure regions (underside) and toward the low pressure regions (upperside). Thus, when the wing is lifting upward, Figure 38, the airfoil section assumes a positive camber distribution that fairs in smoothly with the airfoil's leading edge shape. It should be noted that the actual shape of the Sailwing section is a function of the wind velocity, the wing angle-of-attack, the no-wind airfoil shape, and the amount of tension in the trailing-edge cable. Thus, as the angle-of-attack is increased, thereby increasing the amount of lift that is generated (up until the wing stalls), the resulting

21

increased pressure differential between the upper and lower surfaces causes the amount of camber in the section to increase. This not only causes the maximum value of wing efficiency, lift-to-drag ratio, to occur at fairly high angles-of-attack, but also delays the impending stall, Figure 39. At this point, the importance of maintaining the desired trailing-edge cable tension should be noted. As might be expected, relaxing the cable tension allows for a greater mount of camber and therefore a higher maximum lift coefficient; however, it simultaneously decreases the maximum lift-to-drag ratio obtainable as well as the threshold of critical velocity at which detrimental sail luffing occurs. Thus, the amount of tension in the Sailwing's trailing-edge cable controls the important trade-off between C_{Lmax} and $(L/D)_{max}$. As an upper limit, it might be considered that as the cable tension becomes higher and higher, the Sailwing's behavior becomes more and more like that of a rigid wing.

Another interesting characteristic of the lifting Sailwing is the upward deformation of the trailing-edge in the unsupported mid-span regions of each wing-panel, Figure 40. A result of this action is a reduced angle of attack in these regions and one would expect a local reduction in lift; however, it is generally the case that this effect is more than offset by the increased amount of camber that occurs and results in a locally increased lift generation. In fact, because of this effect, the lift distributions that occur over some Sailwings are often very close to that of the elliptical optimum.

The constant chordwise tension that is a result of the trailing-edge cable and the catenary arc sail cut is responsible for many of the

22

desirable features of the Sailwing over other flexible designs. One such feature is that realtively low drags are present at low angles of attack and lift coefficients. Furthermore, the Sailwing has the ability to pass through the zero-lift angle-of-attack without flapping or luffing. Below the zero-lift angle-of-attack, the asymmetrical pressure distribution on the wing is reversed resulting in the section having negative camber, Figure 41.

All in all, through many years of extensive research, the Sailwing has been found to provide a simple, light-weight and low-cost alternative to the conventional rigid wing while not suffering any performance penalties throughout most low-speed applications.

D) Presentation and Discussion of Test Results

The reduced three-dimensional data taken from the wind-tunnel tests of the eight Sailwing and Sailvane models are presented in the plots of Figures 42-57. For each wing tested, the lift coefficient, drag coefficient, pitching moment coefficient about the quarter-chord point, and lift-to-drag ratio, are plotted as functions of the angle-of-attack of the unloaded mean aerodynamic chord. The significant parameters that have been obtained from these data are summarized in Table III.

It is important to note that a direct comparison of these data to those of a conventional rigid wing is complicated a great deal by the flexible nature of the Sailwing. For example, the Sailwing data is likened to that of a rigid wing in which a movable flap is deflected additionally for each increasing angle of attack increment. This characteristic is responsible for the fact that it is generally impossible in

23

the case of a Sailwing to linearize the drag polar or obtain a meaning-
ful span-efficiency factor as is done from wind-tunnel test data for a
conventional wing. Similarly, it should further be noted that at lower
angles-of-attack (up to approximately five degrees), most Sailwings have
a lift-curve slope which exceeds the theoretical maximum for rigid wings
(2π per radian = .11 per degree). This occurs because the section is
continually varying camber over the angle-of-attack range. At higher
angles-of-attack, the section is unable to deform as much as when it is
less loaded. Therefore, the lift-curve becomes increasingly more like
that of a rigid wing when the angle-of-attack is increased to higher
values.

Section	$dC_L/d\alpha$ (per degree)	α_{L_0}(degree)	C_{Lmax}	$(L/D)_{max}$	$(L/D)C_L=1.0$
Sailvane Model 1	.125	-1.5	1.30	16.0	16.0
Sailvane Model 2	.104	-3.0	1.41	18.0	18.0
Sailvane Model 3	.112	-1.5	.92	12.0	3.6
Semi-Sailwing Model 1	.110	-1.5	1.18	21.0	17.0
Semi-Sailwing Model 2	.098	-2.8	1.47	18.0	17.7
Semi-Sailwing Model 3	.108	-1.0	1.12	13.4	9.0
Sailwing Model 1	.118	- .8	1.30	29.0	27.8
Sailwing Model 2	.118	-2.1	1.49	29.5	27.0

TABLE III: Three-Dimensional Sailwing and Sailvane Aerodynamic
Parameters, Aspect Ratio = 8.4

As previously mentioned, the model tests were conducted using two different trailing-edge cable tension coefficients; however, the data presented is for $C_T = .28$ as the results varied only slightly, in accordance with the expected trends, for $C_T = .07$. It is therefore concluded that for the dynamic pressure at which the tests were performed, both of these values are sufficiently high to allow only minimal increased sail deformation (camber), even at the lower value of C_T.

For the purpose of design, it is often the established procedure in wind-tunnel testing of rigid wings to generate two-dimensional sectional data from three-dimensional data such as that presented for the Sailwing; however, the flexibility of the Sailwing airfoil makes this extremely difficult and the Princeton group does not know of any reasonable method to determine the exact breakdown of total drag into its three-dimensional induced contribution and its two-dimensional profile contribution as this would require that the drag polar be linearized to some degree such that a span efficiency factor could be obtained. As previously mentioned, this is usually not possible in the case of a Sailwing. However, by carefully comparing the information presented in Table I with that of a rigid wing utilizing a similar profile, for example the NACA 4412, it can be realized that the data for the double-membraned Sailwing resembles that of the rigid section to a large extent and it is not at all unreasonable to assume that the Sailwing's two-dimensional characteristics are such that the maximum sectional lift-to-drag ratios are of the same order. Obviously, this approximation leaves a lot to be desired quantitatively; however, the argument is being presented only to give some

25

indication that the sectional efficiency of the Sailwing does not differ significantly from that of a conventional wing section often utilized in windmill-rotor blade design.

E) Conclusions

In examining the data presented in Table III, it becomes clearly evident that the performance penalties paid for deviating from the conventional Sailwing sections are fairly high. In fact, although some reasonably good rotors have been constructed using the single-membraned sail, it seems that some particularly convincing arguments concerning reduced costs and increased simplicity would have to be presented to justify using anything other than the double-membraned cross-sections.

The most outstanding characteris:ic in comparing the effect of the leading-edge shape are the larger values of lift coefficient, along with the associated more abrupt stalling characteristics, that occur with the smaller radius leading-edge. In addition, the smaller radius leading-edge gives rise to a slight shift in the entire lift curve such that a lower angle-of-attack is required to obtain a given lift coefficient.

In considering the application of these sections, the data in Table III demonstrates that the Sailwing's three-dimensional performance is quite competitive with most rigid wings of the same aspect ratio. Thus, the use of the Sailwing should allow the benefits of simpler construction and lower costs to be realized without paying any significant price in performance. In fact, some consideration should be given to the fact that, unlike many of its rigid counterparts, the cambering characteristics found in the Sailwing cause its three-dimensional lift-

26

to-drag ratios to be very near maximum at lift coefficients of close
to 1.0. This situation is probably very close to that which is ideally
desired for optimum windmill rotor performance (Reference 3).

CONCLUDING SUMMARY

1. The Princeton moving-vehicle windmill testing has reached a level of sophistication where it is possible to obtain windmill performance data having both a high degree of repeatability and an acceptable range of experimental scatter with a minimum of effort.

2. The step-by-step geometrical build-up of the 12 ft. diameter, two-bladed Sailwing rotor resulted in the value of the maximum power co-efficient being increased nearly seven times. In addition, a significant amount of information was collected which should prove to be of considerable benefit in furthering the understanding of windmill blade technology.

3. An exploratory research effort to evaluate the concept of a first-stage, co-axial rotor to obtain beneficial aerodynamic interference has found that such a device has either a degrading effect, or no effect what-so-ever, on windmill performance. Thus, it is concluded that future efforts would be more wisely directed toward attempting to optimize the utilization of a center-body assembly.

4. Finally, a comparison based on wind-tunnel studies of various simplified versions of the Sailwing have found the aerodynamic penalties for deviating from the standard cross-section to be quite high. Although it might be possible to justify the use of such sections in limited unique applications (for example, where a low-cost sail reefing capability is a mandatory requirement), in the general case it is more likely that any cost savings would be insignificant when compared to the overall loss in performance.

REFERENCES

1. Sweeney, T. E., et al., <u>Sailwing Windmill Characteristics and Related Topics</u>, Princeton AMS Report No. 1240, Spring, 1975.

2. Blaha, R., <u>The Effect of a Center Body on Axial Flow Windmill Performance</u>, Princeton AMS Report No. 1266, March, 1976.

3. Rohrbach, C., <u>Experimental and Analytical Research on the Aerodynamics of Wind Turbines</u>, Mid-Term Technical Report, ERDA Contract E (11)-2615, February 1976.

APPENDIX I

Contributors

The research discussed in this report has been conducted under
the guidance and supervision of Mr. Thomas E. Sweeney, Director of
Princeton's Flight Concepts Laboratory. Other contributors to the
research effort include Mr. W. B. Nixon, Mr. S. A. Weissenburger,
Mr. R. Blaha, Mr. B. Schrick, and the author, Mr. M. D. Maughmer.

This report has not been distributed by Princeton to anyone
other than the National Science Foundation.

APPENDIX II

Data Correction Technique For Earth Boundary Layer Effect

It has been found by the Princeton group that when the moving-vehicle test facility is used to collect data in the slightly less than ideal conditions of a light wind blowing parallel to the test-track, that the vertical velocity gradient causes two distinct plots to occur, as shown in the sketch, depending on whether the data points were obtained on an upwind or a downwind test pass.
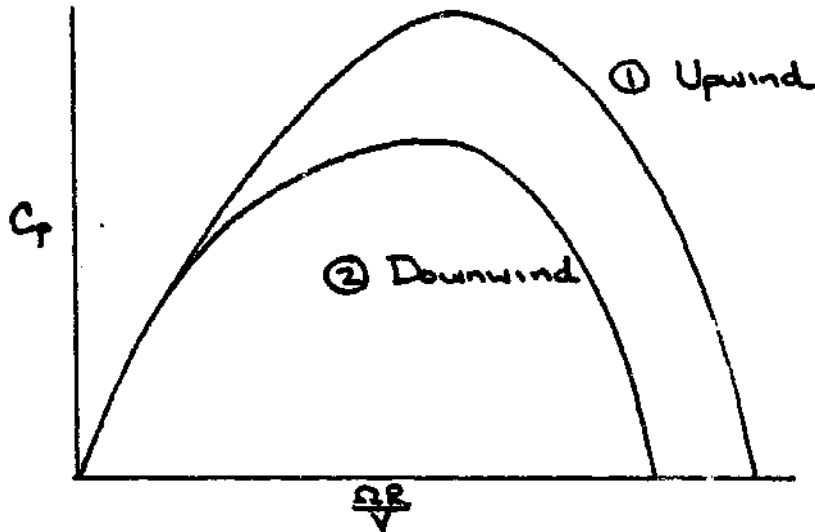
The true windspeed realized by the windmill is actually the indicated airspeed, which is the same for both run directions, modified by a small increment, v , due to the vertical gradient

Upwind: $V_{1\ true} = V_{indicated} + v$

Downwind: $V_{2\ true} = V_{indicated} - v$

Furthermore, the free-wheeling (unloaded) angular velocities of the rotor are not equivalent for the two directions only because the windmill

31

senses two different true windspeeds; however, the free-wheeling tip-speed ratios should (essentially) be equal. Thus, for the no-load condition

$$\frac{\Omega_1 R}{V_{1 \text{ true}}} = \frac{\Omega_2 R}{V_{2 \text{ true}}}$$

where substitution and rearranging yields

$$\frac{\Omega_1}{\Omega_2} = \frac{V_{\text{indicated}} + \nu}{V_{\text{indicated}} - \nu}$$

Solving for ν yields,

$$\nu = (V_{\text{indicated}}) \left\{ \left(\frac{\Omega_1}{\Omega_2} - 1 \right) \Big/ \left(\frac{\Omega_1}{\Omega_2} + 1 \right) \right\}$$

Thus, if the ratio of the upwind to downwind free-wheeling angular velocities is obtained at the initiation of a test series, the increment ν and, therefore, the true wind velocity for each direction can be obtained. If the appropriate true wind velocity value is employed in reducing the data collected, the true performance curve of the windmill should be obtained. As a final note, it should be obvious that this correction procedure assumes the wind velocity to be steady and gust-free throughout the testing. Therefore, it is suggested that the angular-velocity ratio be rechecked during the test period in order to assure that the wind has been reasonably constand and that the correction is valid.

32

FIGURE 1

PRINCETON JEEP WINDMILL TESTING FACILITY
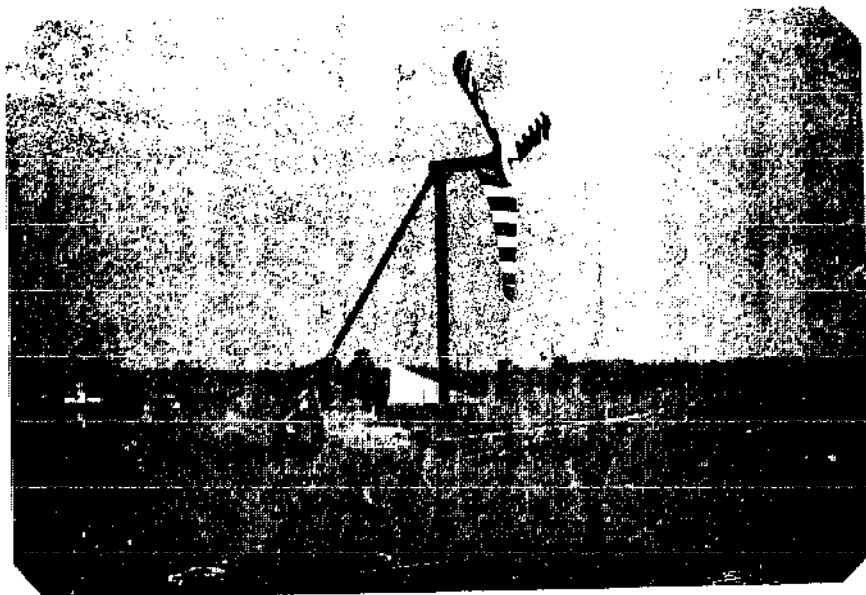
FIGURE 2

PRINCETON JEEP WINDMILL TESTING FACILITY

33

FIGURE 3

34
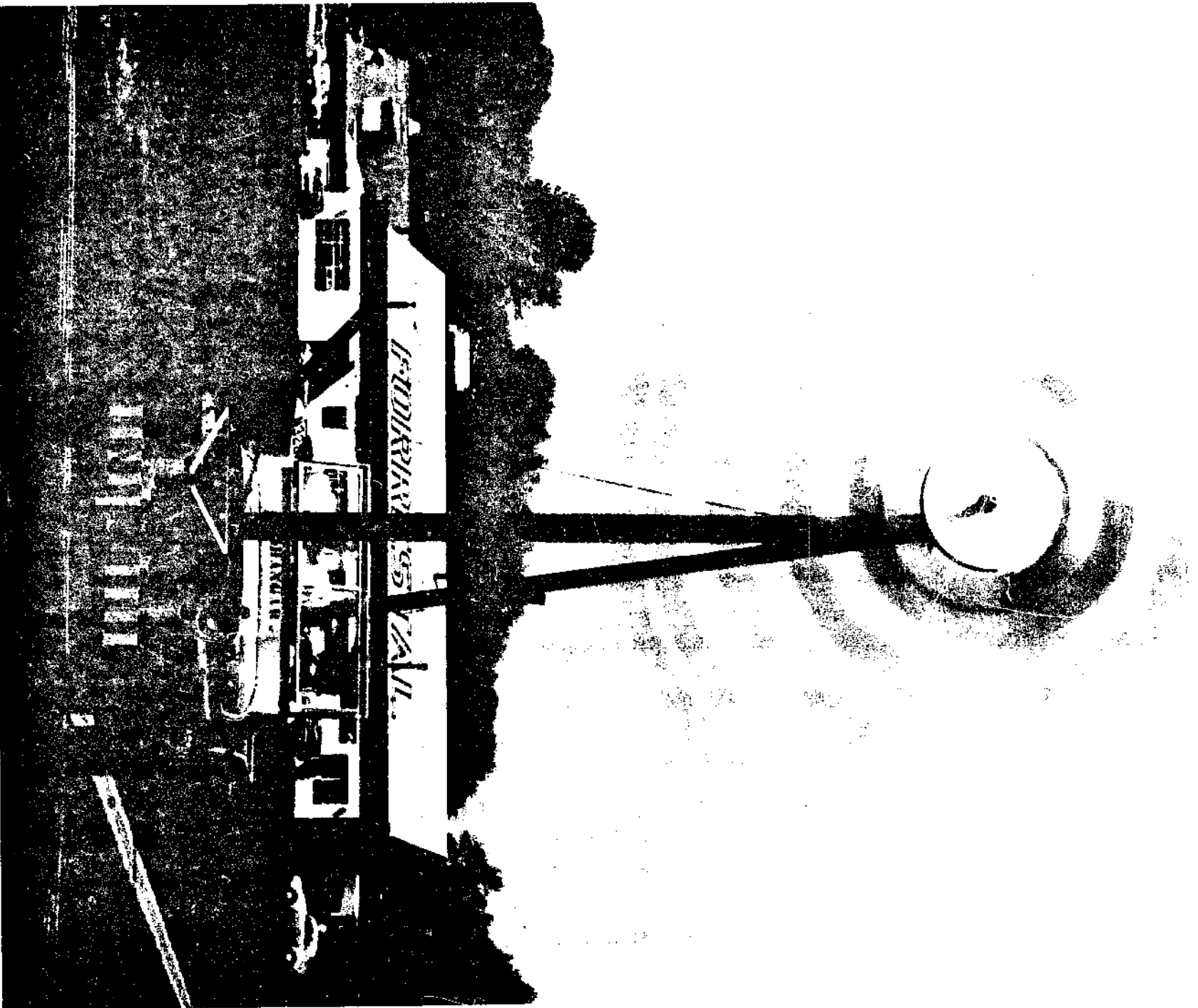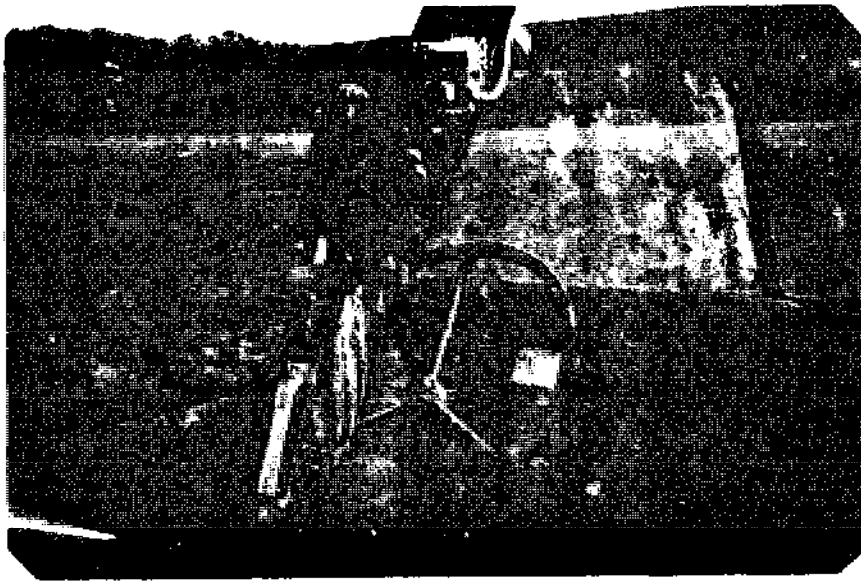
FIGURE 4

ANEMOMETER READ-OUT AND BRAKE ACTUATING MECHANISM
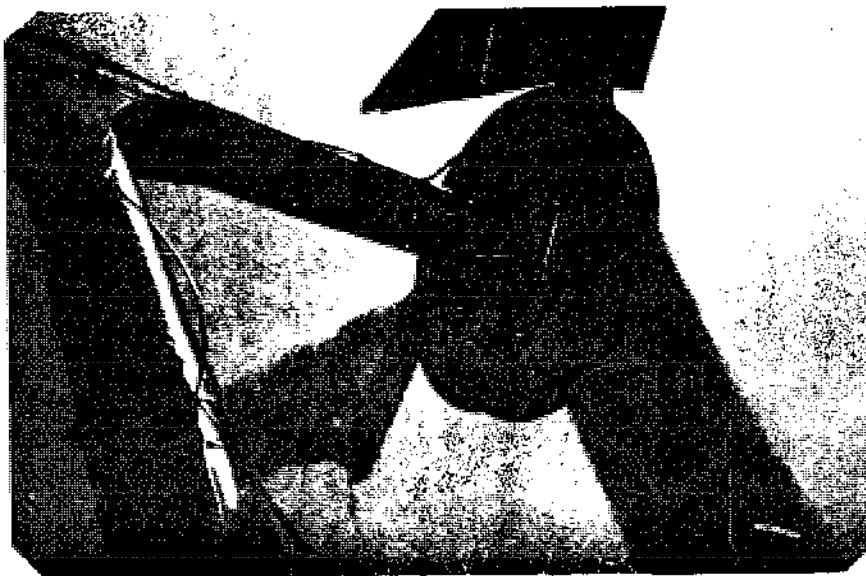
FIGURE 5

DISK-BRAKE ASSEMBLY
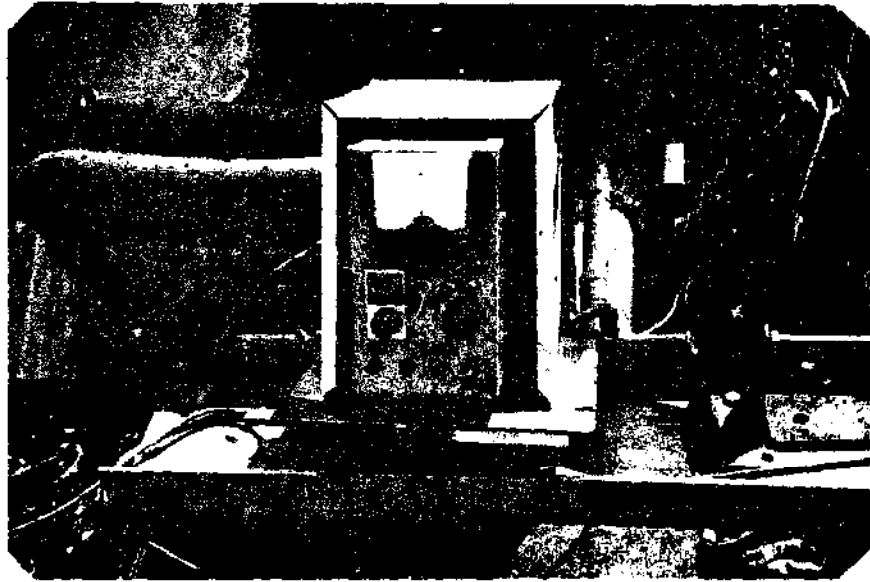
FIGURE 6

TORQUE READ-OUT
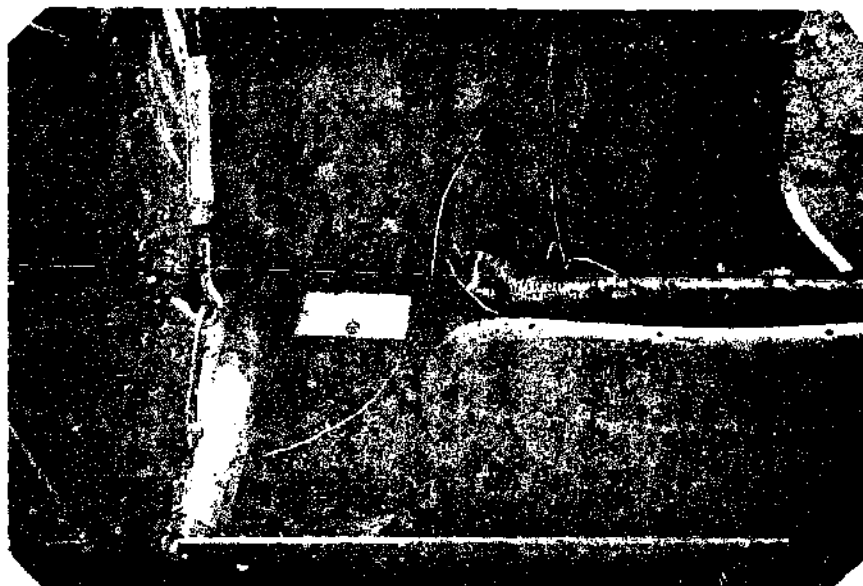
FIGURE 7

ROTOR TACHOMETER READ-OUT

FIGURE 8

DATE: 10-27-75 Wilamette Propeller ... ...

CONFIGURATION: (a) ... R = 6 47 ...

$\beta_{root} = 70°$ $\beta_{tip} = 0°$ $J_{mat} = 20°$

Run	V_∞	N (r/min)	Volts (E)	Torque	Ω (rad/s)	Torque (ft-lb)	M	R
N	4	213	43	0	20.21	0	6.30	0
			36	10	25.71	21.67	5.72	.12
S			40	0	28.57	0	5.96	0
N			41	0	29.27	0	6.01	0
			36	10	25.11	21.67	5.27	.12
			30	20	21.43	43.24	4.40	.20
			23.3	30	16.64	65.01	3.41	.22
S			36	10	25.11	21.67	5.27	.12
			30	20	21.43	43.34	4.40	.20
N			30	20	21.43	43.34	4.40	.20
			27	25	18.57	54.18	3.91	.21
			23.5	30	16.79	65.01	3.44	.23
			20	35	14.75	75.95	2.92	.23
S			26.5	25	18.53	54.18	3.85	.22
			22	30	16.43	.61	3.37	.22
				35			—	—
H			22.3	24	15.5	.61	3.25	.24
			24	30	.5 .5	.61	3.52	.24
			2.1	32	15	.71	3.15	.22
			15	34	13.52	.46	2.78	.21
			15	36	13.57	.61	2.78	.23
S			.5	0	32		5.15	

K•E 10 X 10 TO THE INCH + 7 X 10 INCHES
KEUFFEL & ESSER CO. MADE IN U.S.A.

46 0706

FIGURE 9

FIGURE 10

FIGURE 11

BASIC BLADE PLANFORM

STA. — 0, 0.6', 1, 2', 3', 4', 5', 6'

C × r — .825, 1.25, 2.0, 2.25, 2.50, 2.90, 4.02

Thickness Ratio — .16, .18, .21, .26, .30, .31, .25

CIRCULAR LEADING EDGE

FIGURE 12

(a)

FULL SPAN D-SPAR LEADING EDGE

(b)

FULL SPAN D-SPAR LEADING EDGE
WITH TIP FAIRING

(c)

FULL SPAN D-SPAR LEADING EDGE
WITH TIP FAIRING
WITH 20% CENTER BODY

(d)

FULL SPAN D-SPAR LEADING EDGE
WITH TIP FAIRING
WITH MID SPAN STIFFNER

(e)

FULL SPAN D-SPAR LEADING EDGE
WITH TIP FAIRING AND MID-SPAN RIB

(f)

FULL SPAN D-SPAR LEADING EDGE
WITH TIP FAIRING AND MID-SPAN RIB
WITH 20% CENTER BODY

(g)

The Several Blade Planforms Tested - Full Scale

41

K•E 10 X 10 TO THE INCH • 7 X 10 INCHES
KEUFFEL & ESSER CO. MADE IN U.S.A.

46 0706

FIGURE 13

K·E 10 X 10 TO THE INCH • 7 X 10 INCHES
KEUFFEL & ESSER CO. MADE IN U.S.A.

46 0706.

FIGURE 14

K·E 10 X 10 TO THE INCH • 7 X 10 INCHES
KEUFFEL & ESSER CO. MADE IN U.S.A.

46 0706

FIGURE 15

K·E 10 X 10 TO THE INCH · 7 X 10 INCHES
KEUFFEL & ESSER CO. MADE IN U.S.A.

46 0706 ·

CONFIG. (c₂)
$V = 19.6$ FT/SEC
● $\beta_{ROOT} = +10°$
▲ $\beta_{ROOT} = +15°$
■ $\beta_{ROOT} = +30°$
TWIST = 30°

FIGURE 16

K•E 10 X 10 TO THE INCH • 7 X 10 INCHES
KEUFFEL & ESSER CO. MADE IN U.S.A.

46 0706

FIGURE 17

10 X 10 TO THE INCH • 7 X 10 INCHES
KEUFFEL & ESSER CO. MADE IN U.S.A.

46 0706

FIGURE 78

C_p : POWER COEFFICIENT

ψ : TIP-SPEED RATIO

OGIVE (C_d)
$V = 1016$ FT/SEC
$\beta_{ROOT} = 17.5°$
TWIST = 30°

K•E 10 X 10 TO THE INCH • 7 X 10 INCHES
KEUFFEL & ESSER CO. MADE IN U.S.A.

46 0706

FIGURE 19

K&E 10 X 10 TO THE INCH • 7 X 10 INCHES
KEUFFEL & ESSER CO. MADE IN U.S.A.

CONFIG: (e)
V = 19.6 Ft/Sec
• ßroot = +10°
▲ ßroot = +20°
TWIST = 20°

C_P

POWER
COEFFICIENT

μ. TIP-SPEED RATIO

FIGURE 20

K·E 10 X 10 TO THE INCH · 7 X 10 INCHES
KEUFFEL & ESSER CO. MADE IN U.S.A.

46 0706

FIGURE XI

CONFIG. (C) WITH
2.0% CENTERBODY
V = 19.6 FT/SEC
▲ β_root = +15°
■ β_root = +20°
TWIST = 30°

C_p

POWER
COEFFICIENT

.5
.4
.3
.2
.1
0

0   1.0   2.0   3.0   4.0   5.0   6.0   7.0   8.0

μ TIP-SPEED RATIO

FIGURE 82

CONFIG. (2) WITH
20% CENTERBODY
$V = 31.3$ FT/SEC.
▲ $\beta_{root} = +15°$
■ $\beta_{root} = +20°$
TWIST = 20°

POWER
COEFFICIENT

C_p

.5

.4

.3

.2

.1

0

0   10   20   30   40   50   60   70   80

μ : TIP-SPEED RATIO

FIGURE 23

K+E 10 X 10 TO THE INCH • 7 X 10 INCHES
KEUFFEL & ESSER CO. MADE IN U.S.A.

46 0706

FIGURE 24

Power Coefficient vs. Tip-Speed Ratio plot. Axes: vertical C_P (Power Coefficient) from 0 to .5; horizontal μ : TIP-SPEED RATIO from 0 to 8.0. Legend: CONFIG. CE.I, $V = 37.3$ Ft/Sec, $\beta_{root} = +5°$, $\beta_{root} = +10°$, $\beta_{root} = +15°$, TWIST = 2.0°.

Figure 25

K•E 10 X 10 TO THE INCH • 7 X 10 INCHES
KEUFFEL & ESSER CO. MADE IN U.S.A.

46 0706

CONFIG. (5)
$V = 31.3$ FT/SEC
$B/8_{max} = 10°$
TWIST = 20°

C_p

POWER
COEFFICIENT

λ: TIP-SPEED RATIO

FIGURE 26

FIGURE 27

JEEP WINDMILL TESTING FACILITY AND CO-AXIAL

WINDMILL ROTOR ASSEMBLY

FIGURE 28

CLOSE-UP OF THE CO-AXIAL WINDMILL ROTOR ASSEMBLY

K·E 10 X 10 TO THE INCH · 7 X 10 INCHES
KEUFFEL & ESSER CO. MADE IN U.S.A.

46 0706

CONFIG: CO-AXIAL WINDMILL
BASELINE (J) MINUS TIPS
$V = 37.5$ Ft/sec.
$\beta_{.75R} = +15°$
TWIST = 20°

C_p

POWER
COEFFICIENT

$\mathcal{M} :$ TIP-SPEED RATIO

FIGURE 29

K•E 10 X 10 TO THE INCH • 7 X 10 INCHES
KEUFFEL & ESSER CO. MADE IN U.S.A.

46 0706

FIGURE 30

FIGURE 37

CONFIG: CO-AXIAL WINDMILL
C₂ SYNCHRONIZED
FULL BRAKING

V = 31.3 Ft/Sec.

FIGURE 32

CONFIG: CO-AXIAL WINDMILL
COUNTER-ROTATING

$V = 37.3$ FT/SEC.

$\beta_{3/4} = +15°$

TWIST $= 20°$

$\beta_{LOWER}_{ROTOR} = +20°$

POWER COEFFICIENT

C_P

λ, TIP-SPEED RATIO

FIGURE 33

K·E 10 X 10 TO THE INCH • 7 X 10 INCHES
KEUFFEL & ESSEN CO. MADE IN U.S.A.

46 0706

CONFIG : CO-AXIAL WINDMILL
COUNTER-ROTATING

$V = 37.3$ FT/SEC

● $\beta_{ROOT} = +75°$

TWIST = 20°

β UPSTREAM = +5°
ROTOR

C_P

POWER
COEFFICIENT

.5

.4

.3

.2

.1

0

0   1.0   2.0   3.0   4.0   5.0   6.0   7.0   8.0

η : TIP-SPEED RATIO

FIGURE 34

SAILVANE MODEL 1

SAILVANE MODEL 2

SAILVANE MODEL 3

SEMI-SAILWING MODEL 1

SEMI-SAILWING MODEL 2

SEMI-SAILWING MODEL 3

SAILWING MODEL 1

SAILWING MODEL 2

FIGURE 35

SAILVANE AND SAILWING CROSS-SECTIONS TESTED IN THE WIND-TUNNEL

SPAN = 37.8"

AREA = 1.17 ft.^{2}

SCALE 1/2" = 1.0"

$\overline{C}_A$

SAILVANE, SEMI-SAILWING AND SAILWING PLANFORMS

$$M.A.C. = \overline{C}_A = \frac{\int_{-s}^{+s} C^2 dy}{\int_{-s}^{+s} C\, dy} = .44\ ft.^3 \Big/ {}_{1.17\ ft.^2} = .376\ ft. = 4.5"$$

ASPECT RATIO = 8.5

37.8"

6.8"

3.9"

MODEL DIMENSIONS

SAILVANE, SEMI-SAILWING AND SAILWING PLANFORM

SCALE 1/4" = 1.0"
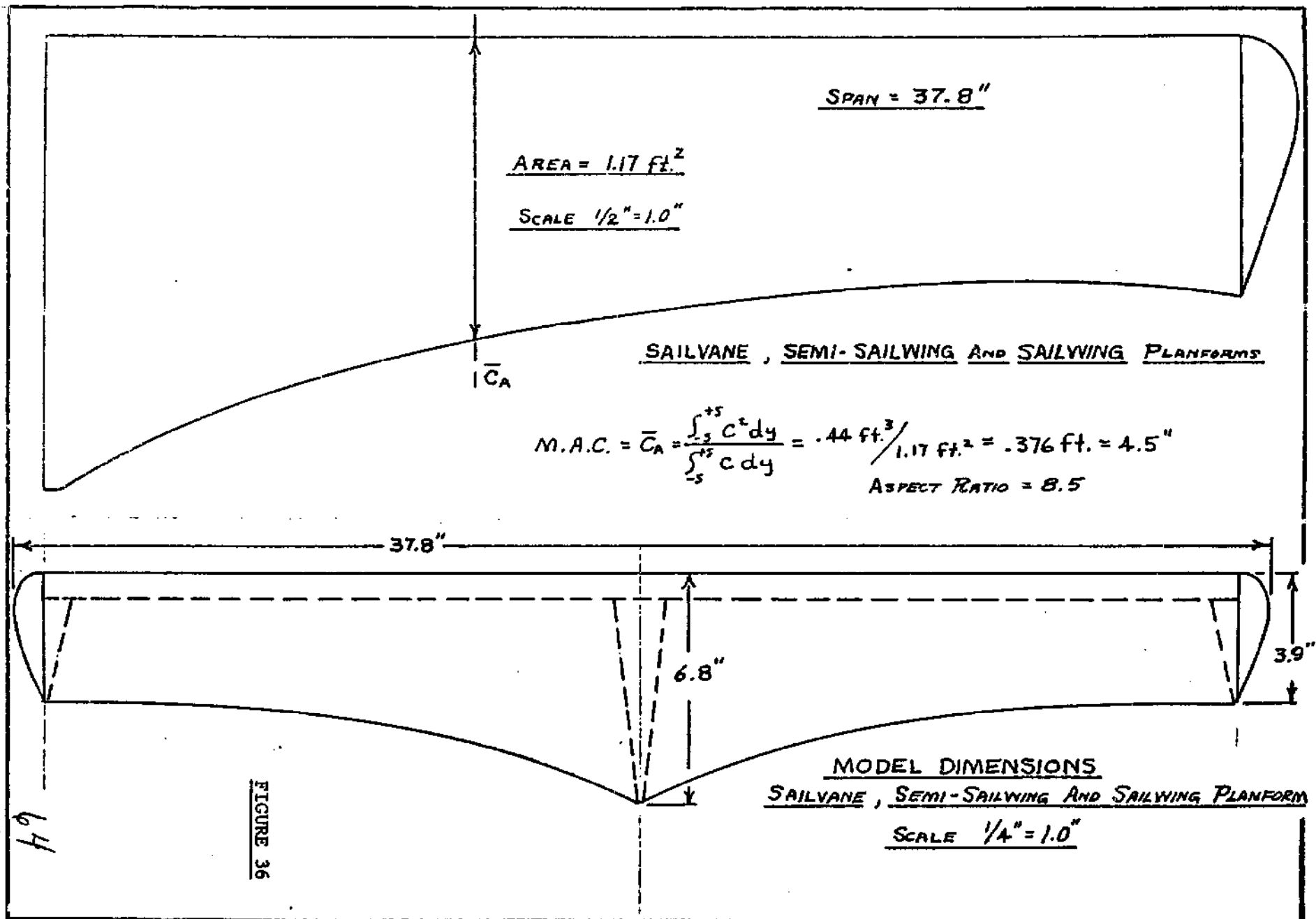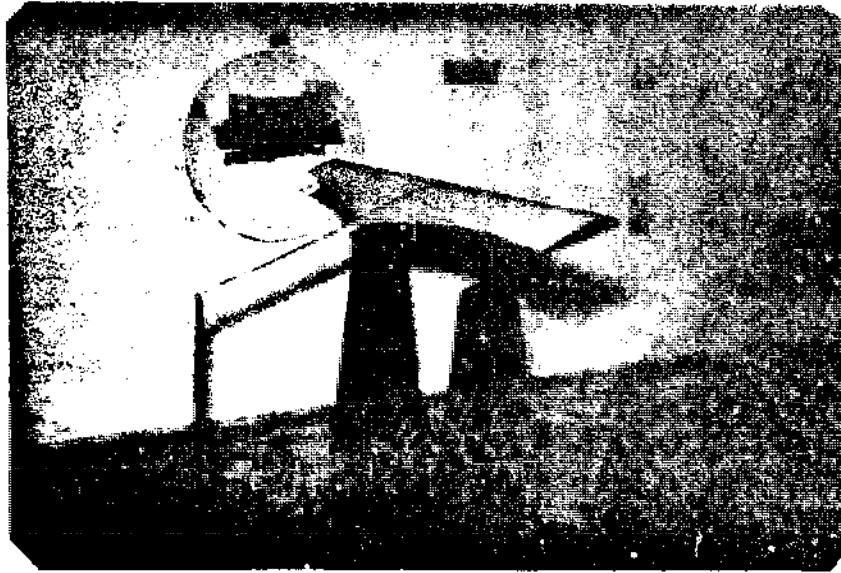
FIGURE 36

FIGURE 37

UNLOADED SAILVANE MOUNTED IN WIND-TUNNEL

(NO WIND)
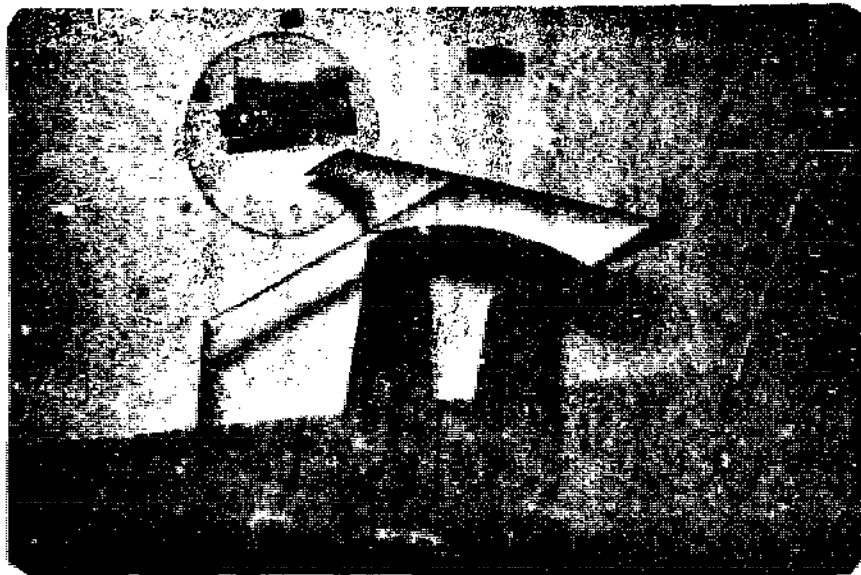
FIGURE 38

LOADED SAILVANE

65
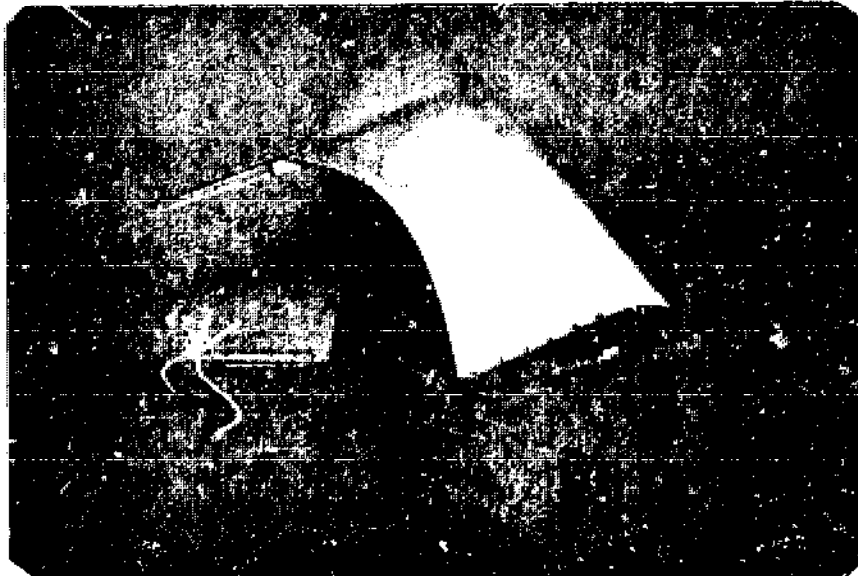
FIGURE 39

SAILVANE POSITIVELY
CAMBERED IN A LIFTING
CONDITION

FIGURE 40

PHOTO SHOWING TRAILING
EDGE DEFORMATIONS
UNDER LOAD

FIGURE 41

SAILVANE IN A NEGATIVE
LIFTING CONDITION

SAILVANE MODEL 1   FIGURE 42

SAILVANE MODEL 1

FIGURE 43

SAILVANE MODEL 2   FIGURE 44

SAILVANE MODEL 2

FIGURE 45
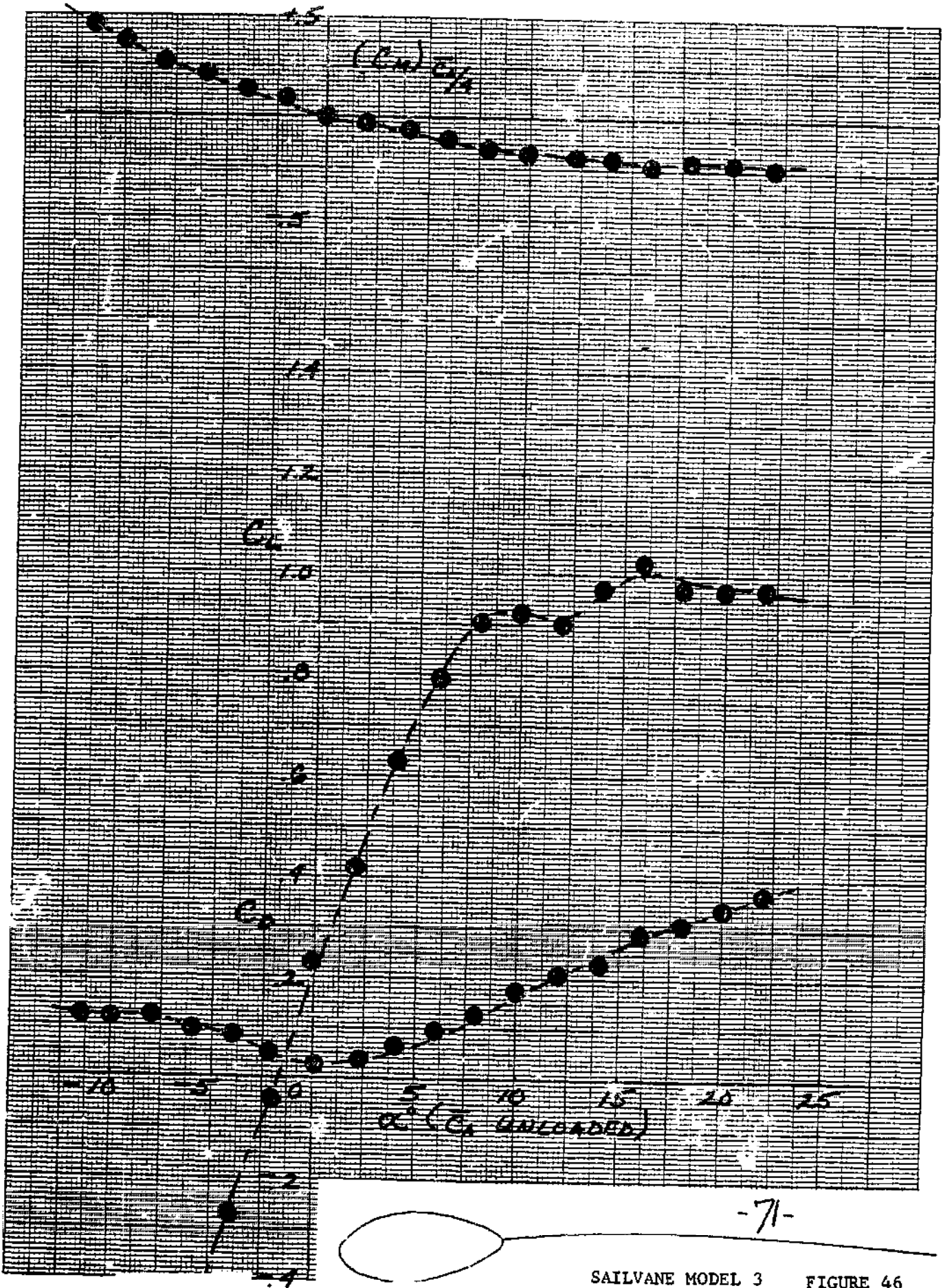
SAILVANE MODEL 3   FIGURE 46

SAILVANE MODEL 3   FIGURE 47

72
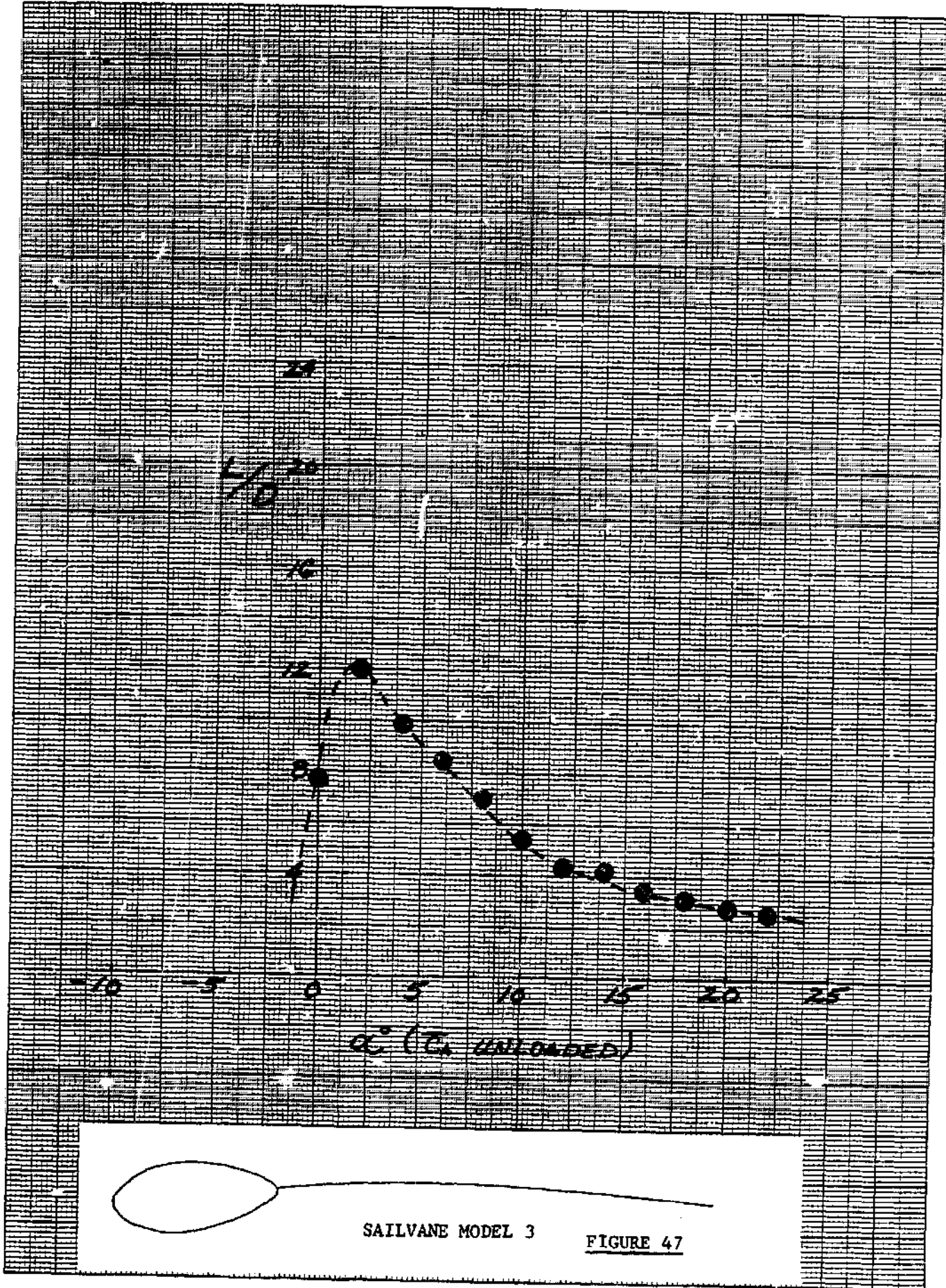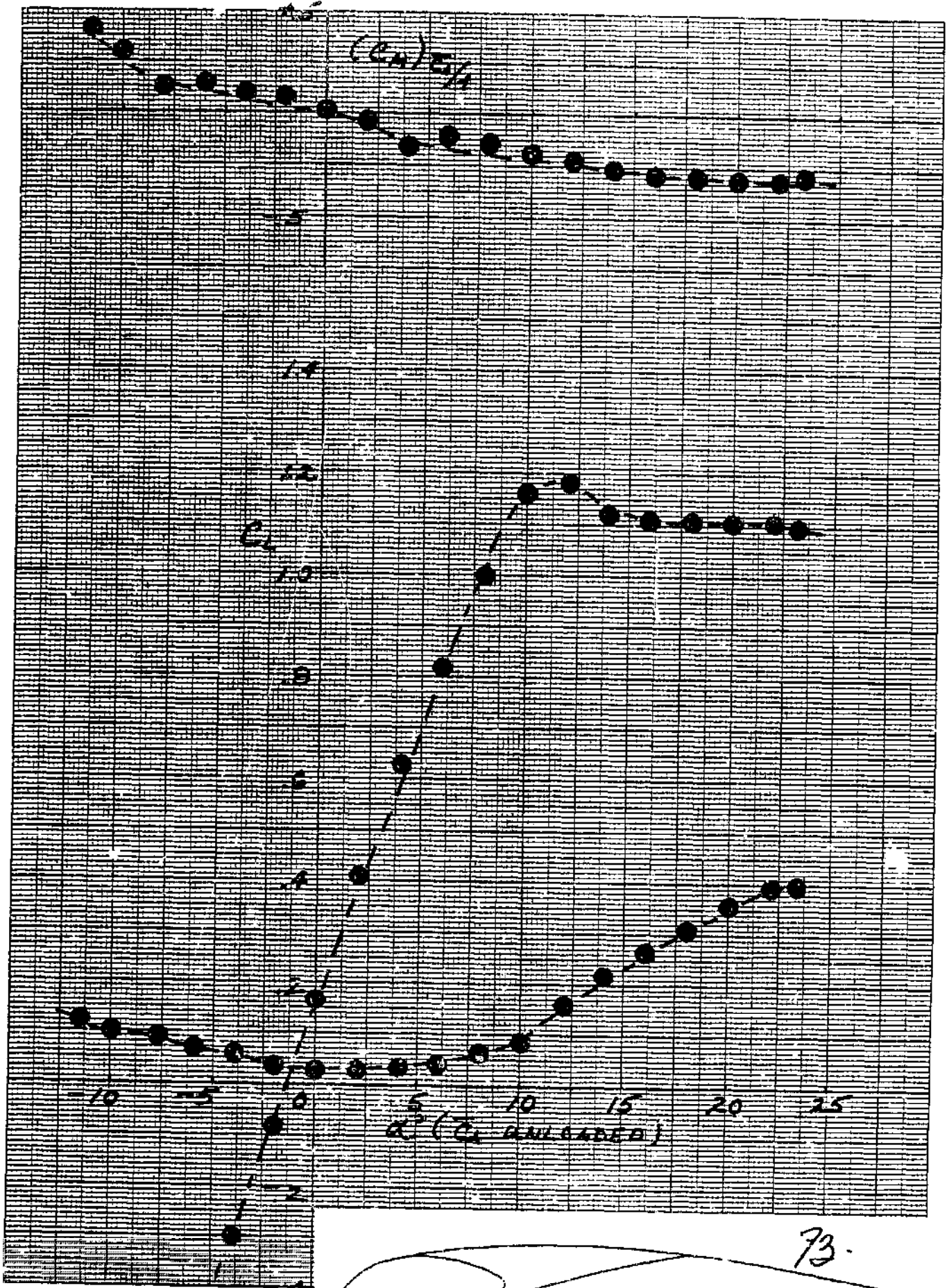
SEMI-SAILWING MODEL 1   FIGURE 48
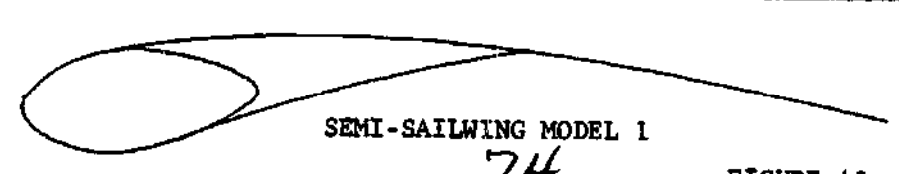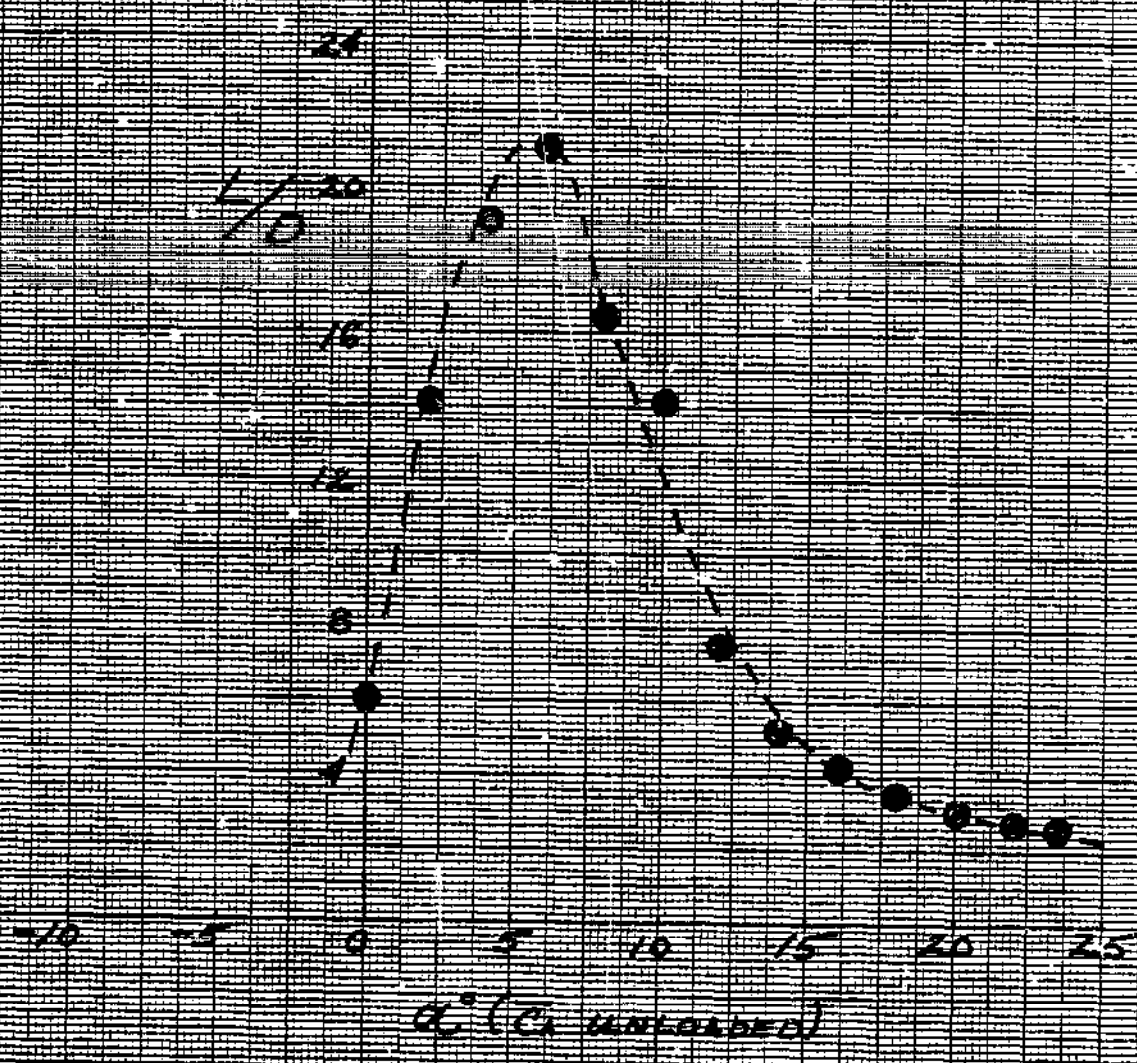
SEMI-SAILWING MODEL 1

74

<u>FIGURE 49</u>

SEMI-SAILWING MODEL 2   <u>FIGURE 50</u>

-75-

SEMI-SAILWING MODEL 2

-76-
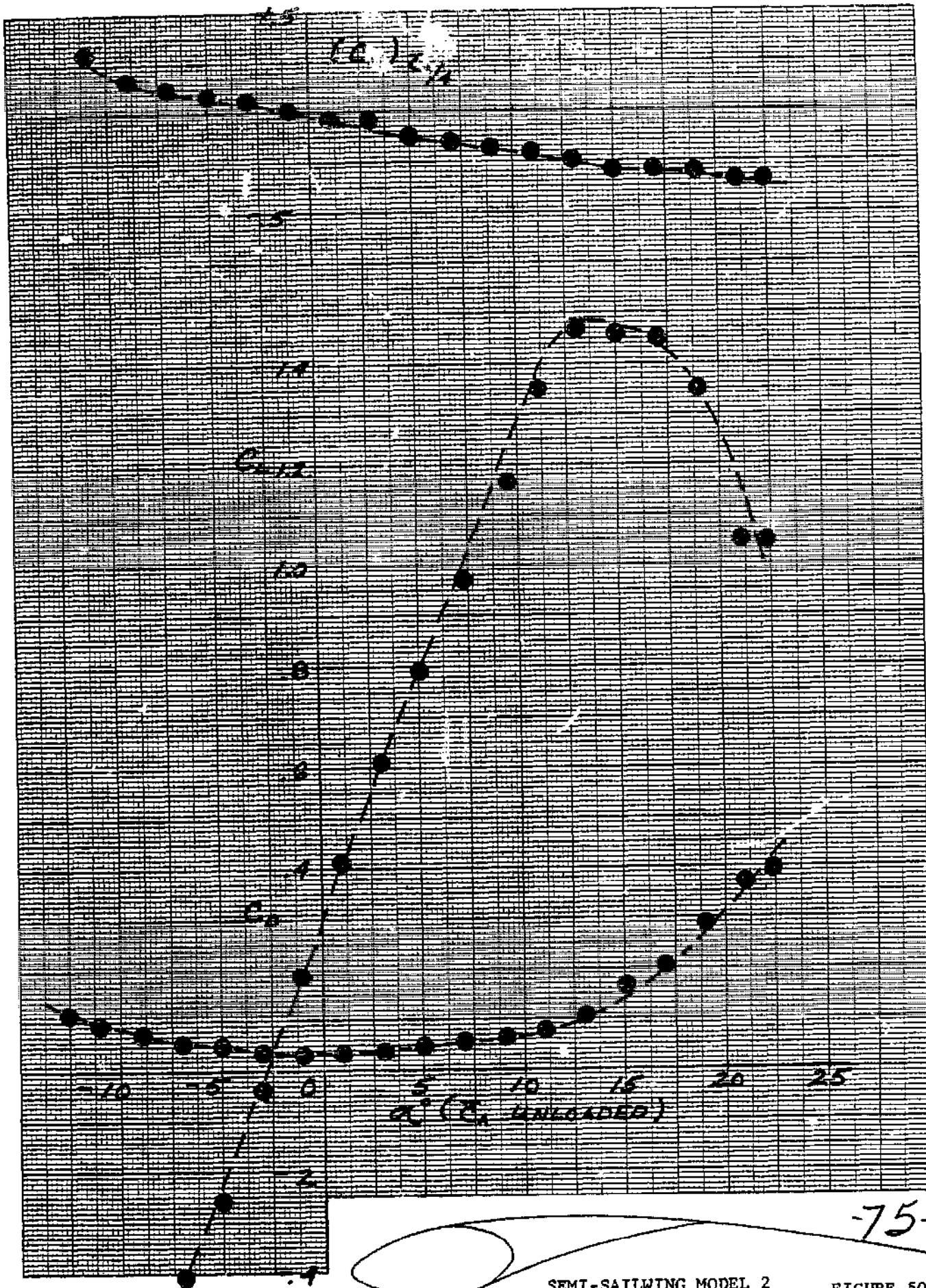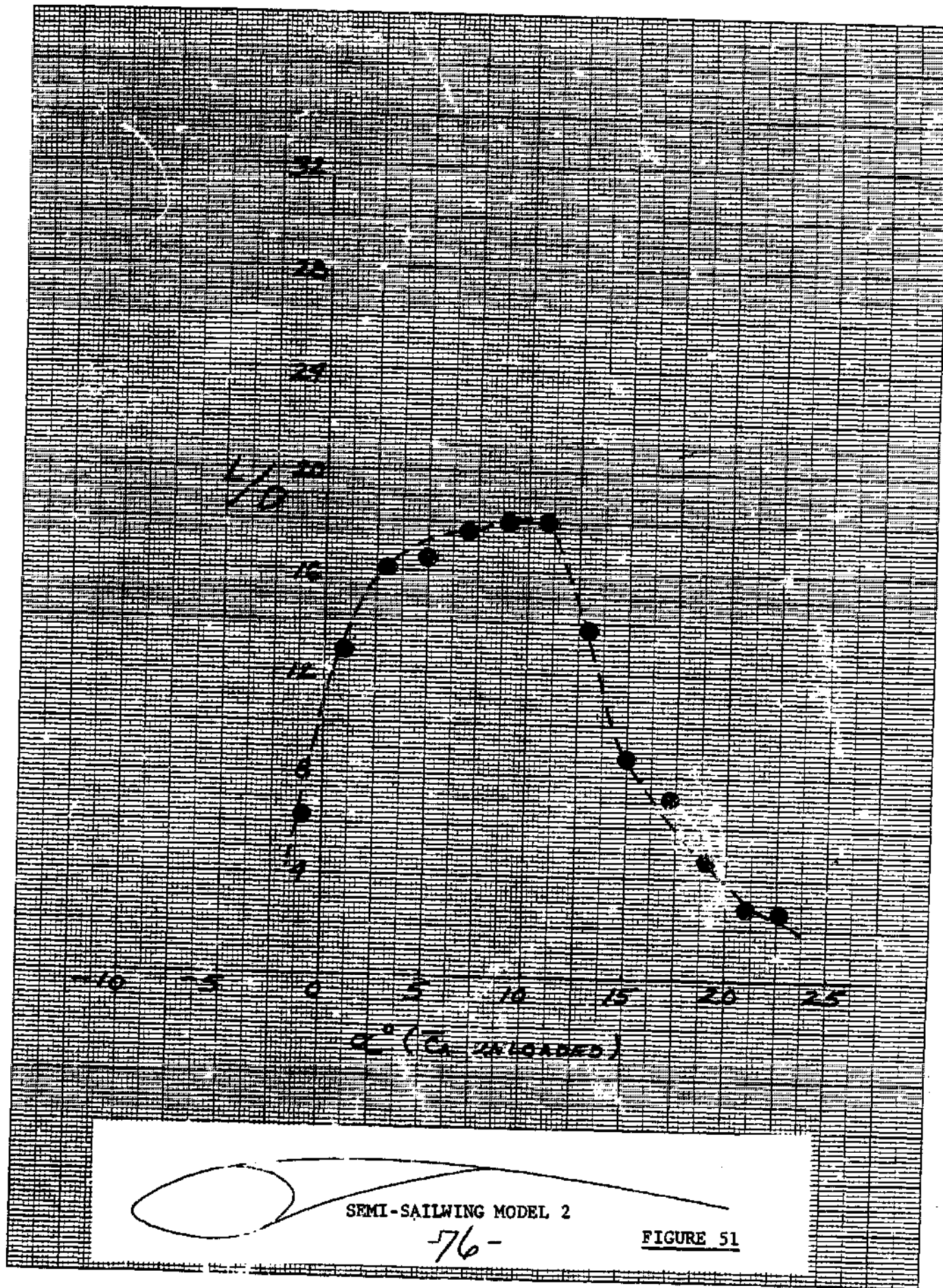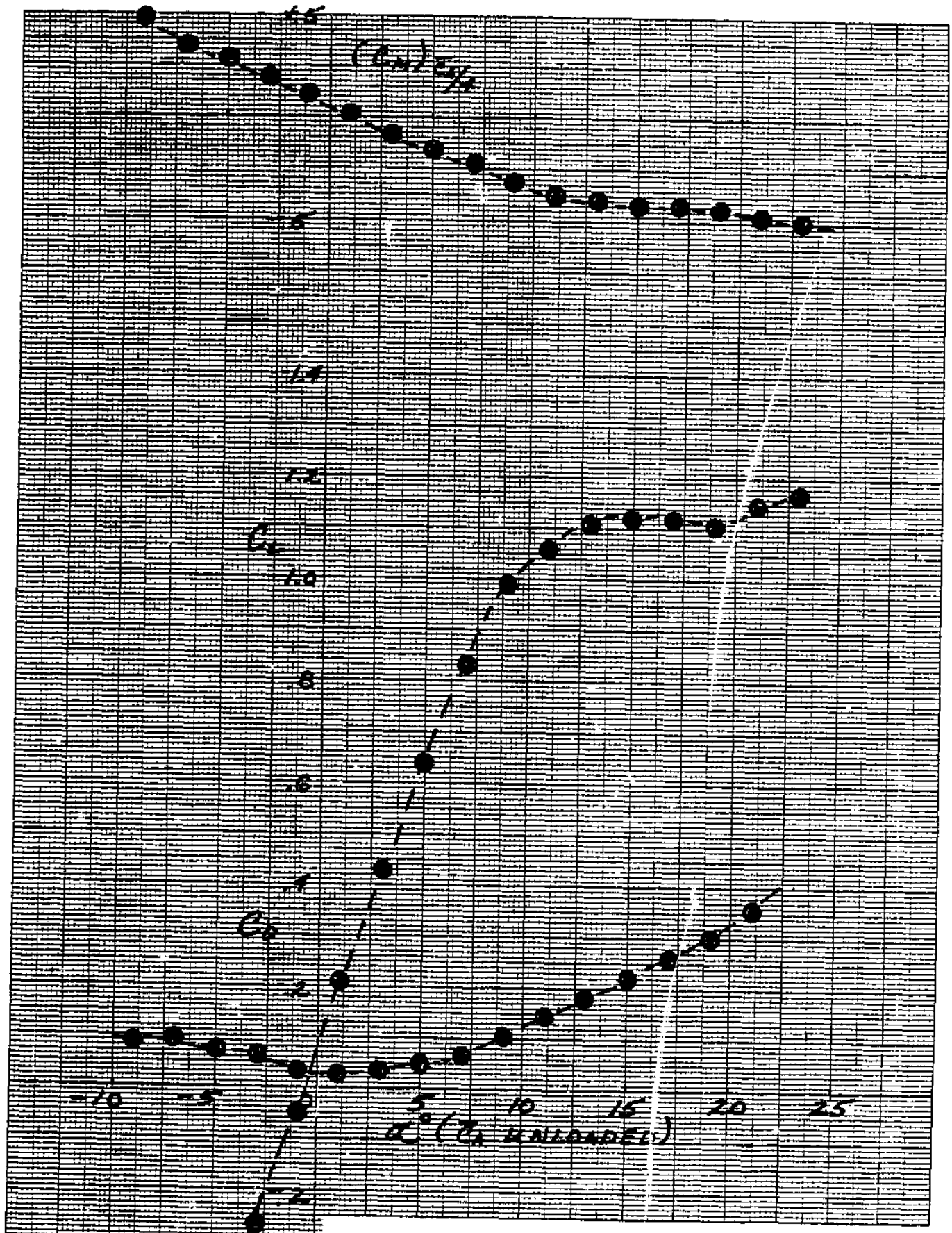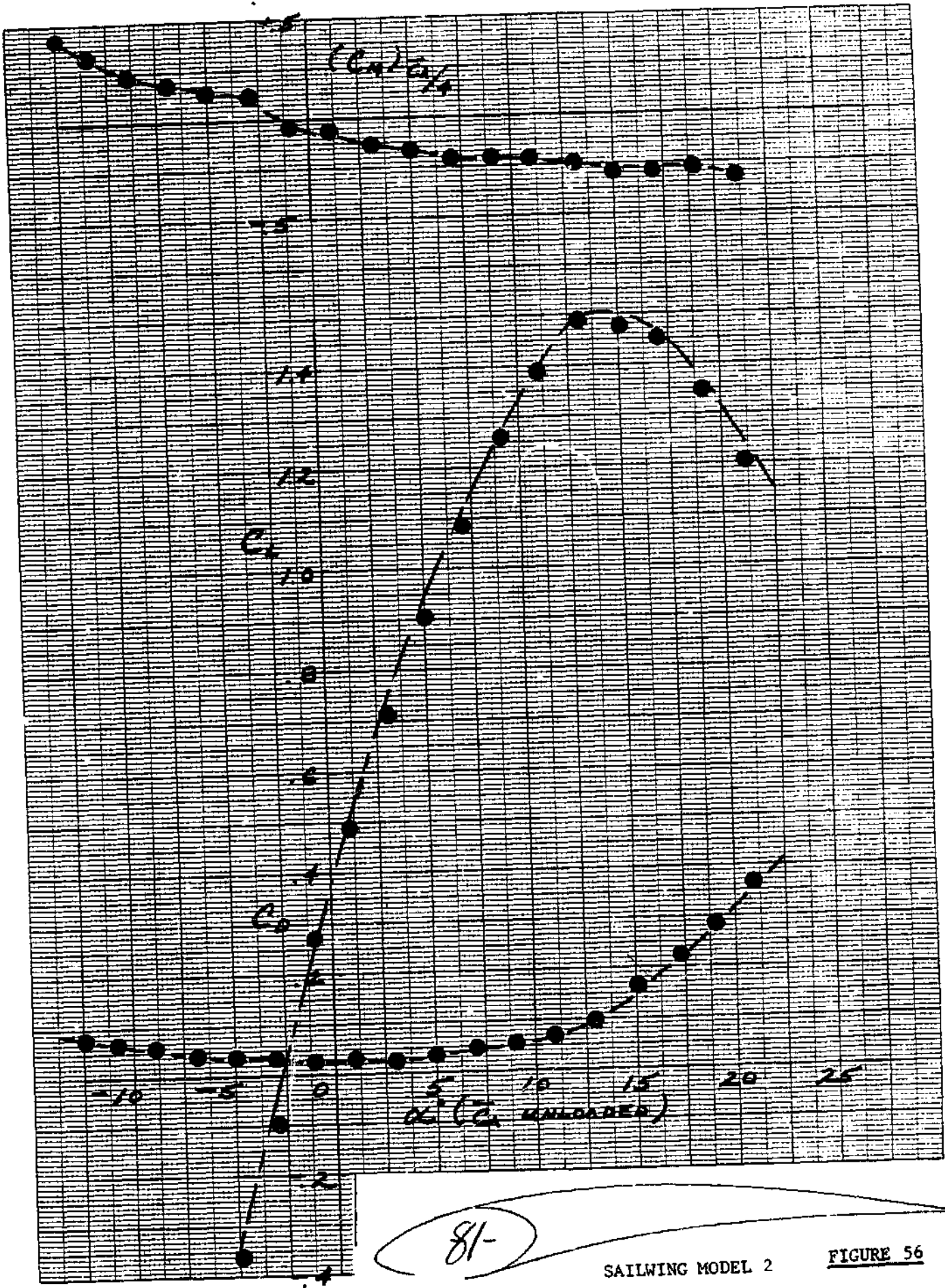
FIGURE 51

FIGURE 52

SEMI-SAILWING MODEL 3

SAILWING MODEL 1   FIGURE 54

79

SAILWING MODEL 1   FIGURE 55

SAILWING MODEL 2   FIGURE 56

SAILWING MODEL 2

FIGURE 57

82